Draft – Discriminating Seagrasses From Green Macroalgae in European Intertidal areas using high resolution multispectral drone imagery – Draft

Simon Oiry[a,*], Bede Ffinian Rowe Davies[a], Ana I. Sousa[b], Philippe Rosa[a], Maria Laura Zoffoli[c], Guillaume Brunier[d], Pierre Gernez[a], Laurent Barillé[a]

[a] *Institut des Substances et Organismes de la Mer, ISOMer, Nantes Université, UR 2160, F-44000 Nantes, France,*

[b] *ECOMARE - Laboratory for Innovation and Sustainability of Marine Biological Resources, CESAM – Centre for Environmental and Marine Studies, Department of Biology, University of Aveiro, Campus Universitário de Santiago, 3810-193 Aveiro, Portugal,*

[c] *Consiglio Nazionale delle Ricerche, Istituto di Scienze Marine (CNR-ISMAR), 00133 Rome, Italy,*

[d] *BRGM French Geological Survey, Cayenne 97300, French Guiana,*

Abstract

Coastal areas support seagrass meadows, which offer crucial ecosystem services including erosion control and carbon sequestration. However, these areas are increasingly impacted by human activities, leading to habitat fragmentation and seagrass decline. In situ surveys, traditionally performed to monitor these ecosystems face limitations on temporal and spatial coverage, particularly in intertidal zones, prompting the addition of satellite data within monitoring programs. Yet, satellite remote sensing can be limited by too coarse spatial and/or spectral resolution, making it difficult to discriminate seagrass from other macrophytes in highly heterogenous meadows. Drone (unmanned aerial vehicles – UAV) images at a very high spatial resolution offer a promising solution to address challenges related to spatial heterogeneity and intrapixel mixture. This study focuses on using drone acquisitions with a ten spectral band sensor similar to that onboard Sentinel-2, for mapping intertidal macrophytes at low tide (i.e. during a period of emersion) and effectively discriminating between seagrass and green macroalgae. Nine drone flights were conducted at two different altitudes (12 m and 120 m) across heterogeneous intertidal European habitats in France and Portugal, providing multispectral reflectance observation at very high spatial resolution (8 mm and 80 mm respectively). Taking advantage of their extremly high spatial resolution; the low altitude flights were used

*Corresponding author
Email address: `oirysimon@gmail.com` (Simon Oiry)

to train a Neural Network classifier to discrimintate five taxonomic classes of intertidal vegetation: Magnoliopsida (Seagrass), Chlorophyceae (Green macroalgae), Phaeophyceae (Brown algae), Rhodophyceae (Red macroalgae) and benthic Bacillariophyceae (Diatoms), and validated using concomitant field measurements. Classification of drone imagery resulted in an overall accuracy of 94% across all sites and images, covering a total area of 467 000 m². The model exhibited an accuracy of 96.4% in identifying seagrass. In particular , seagrass and green algae can be discriminated. The very high spatial resolution of the drone data made it possible to assess the influence of spatial resolution on the classification outputs, showing a limited loss in seagrass detection up to about 10m. Altogether, out findings suggest that the Multi-Spectral Instrument (MSI) onboard Sentinel-2 offers a relevant trade-off between its spatial and spectral resolution, thus offering promising perspectives for satellite remote sensing of intertidal biodiversity over lager scales.

Keywords: Drone, Remote Sensing, Seagrass, Coastal Ecosystems, Neural Network

1. Introduction

Coastal areas are vital hotspots for marine biodiversity, with intertidal seagrass meadows playing a crucial role at the interface between land and ocean [1]. Seagrass meadows provide a myriad of ecosystem services, including carbon sequestration, oxygen production, protection against sea-level rise and coastline erosion, and mitigation of eutrophication [1, 2]. They serve as vital habitats for a diverse array of marine and terrestrial species, providing living, breeding, and feeding grounds [3, 4, 5]. Due to the concentration of human activities in coastal zones, seagrass meadows are directly exposed to and impacted by anthropogenic pressures. Global regression and fragmentation of seagrass meadows are currently observed due to climate change, diseases, urbanization, land reclamation, dredging, competition with alien species, and reduction in water quality [6, 7, 8, 9, 10, 11, 12, 2]. Both habitat fragmentation and reduction, in turn, can severely compromise the effectiveness of ecosystem services provided by seagrass meadows. While improvements in water quality and hydrodynamics have been recently reported in Europe, allowing an overall recovery of seagrass ecosystems at local and European scales, many coastal waters worldwide are still subjected to strong eutrophication processes [13, 14, 2]. Coastal eutrophication has been associated to excessive accumulation of green macroalgae, so-called green tides [15]. Green tides produce shade and suffocation over seagrass individuals, thus threatening the health of seagrass ecosystems [16].

The importance of seagrass meadows and the variety of ecosystem services they provide have led to the enhancement of both global and regional programs to monitor Essential Oceanic Variable (EOVs) such as seagrass composition [17], as well as Essential Biodiversity Variable (EBVs) such as seagrass taxonomic diversity, species distribution, population abundance, and phenology [18]. Traditionally, indicators of seagrass status have been quantified using *in situ* measurements. However, the acquisition of field measurements in intertidal zones is notoriously challenging. Intertidal seagrass meadows are only exposed during low tide and can be situated in difficult-to-reach mudflats, potentially leading to inaccurate and limited estimations with conventional sampling techniques [19]. Satellite observations have been proven effective in complementing *in situ* sampling, allowing for near real-time and consistent retrieval of seagrass EOVs and EBVs over extensive meadows [14, 20, 21, 22, 23, 24].

While satellite remote sensing (RS) provides temporally consistent observations over large spatial scales, its utilization over intertidal areas is limited by several constraints. Satellite missions with a high temporal resolution (e.g. daily MODIS observation) are limited by too coarse spatial resolution (>100 m) to accurately map patchy seagrass meadows. Missions with a high spatial resolution such as Sentinel-2 (10 m) or Landsat8/9 (30 m) can be limited by low spectral resolution. The limited number of spectral bands challenges accurate discrimination of seagrass from other co-existing macrophytes. In particular, Chlorophyceae (green algae) and marine Magnoliopsida (seagrass) share the same pigment composition [25, 26], resulting in a similar spectral signature in terms of reflectance, especially in the visible range [27, 28]. Recently, using advanced machine-learning algorithms trained with a large hyperspectral library of more than 300 field reflectance spectra, [27] demonstrated that it was possible to discriminate Magnoliopsida from Chlorophyceae using reflectance spectra at Sentinel-2 's spectral resolution. However the application of this approach to satellite RS remains to be validated. Moreover patches of green algae can develop at small spatial scales that are not observable using Sentinel-2 and/or Landsat-8/9 images [29], especially during the initial stage of a green tide.

Drones (Unmanned Aerial Vehicles – UAVs) can potentially fill the data gaps left by satellite RS and *in situ* measurements, due to their ability to provide spatially-explicit observations at very high spatial resolutions (pixel size from mm to cm) while capturing data at multi-spectral resolution [30, 31]. The versatility of drones allows for their application across a diverse thematic range , from coastal zone management [32, 33, 34] to mapping species distribution [35, 36, 37, 38, 39, 2]. However, when applied to coastal habitat mapping, previous case studies were mostly limited to a low number of **drone** flights over a single study site, restricting the generalizability of their application over wider geographical scales [38, 40, 41, 39]. **These studies have demonstrated the capability of drones to map intertidal habitats, including seagrasses; however, broader generalization of these findings is still lacking. The current paper uniquely expands the spatial and methodological scope of drone-based remote sensing for intertidal habitat mapping across a broad biogeographical range. It demonstrates the feasibility of accurately classifying diverse macrophyte types across various study sites, with a particular focus on distinguishing Magnoliopsida (seagrasses) and Chlorophyceae (green algae). Unlike previous studies, our approach integrates multiple spatial scales by simulating satel-**

lite resolutions and quantifying the impact of spatial resolution on classification accuracy. Nine drone flights were performed over soft-bottom intertidal areas along the Atlantic coastlines of two European countries (France and Portugal), covering a wide range of habitats, from monospecific seagrass meadows to meadows mixed with green, or red macroalgae. A deep learning algorithm was trained and validated for macrophyte discrimination, emphasizing applicability across diverse sites without a loss of prediction accuracy. The classification maps obtained at a very high spatial resolution with the drone were spatially degraded to satellite resolutions, making it possible to assess the effect of spatial resolution on classification accuracy, and provide insights for coastal habitat mapping using satellite remote sensing. **This study is, therefore, among the first to quantify the effects of spatial resolution on the accuracy of drone-based macrophyte classification across a wide geographical scale, providing a framework for to better understand satellite-based classification challenges.**

2. Material & Methods

2.1. Study sites

Seven study sites distributed between France and Portugal were selected for their extensive intertidal seagrass beds. Two sites were located in the Gulf of Morbihan, France (Figure 1 A : 47.5791°N, 2.8018°W). This gulf covers an area of 115 km² and is only connected to the sea through a 900 m wide channel. A total of 53 small islands are scattered across the gulf leading to 250 km of shorelines. Patchy seagrass meadows can be found on many of these islands. One of the sites within the gulf was on one its islands (Arz) and the other was located further south on a mainland beach area (Duer). The Gulf of Morbihan is a Natura 2000 site and a Regional Protected Area due to its rich biodiversity, including its seagrass meadows, and is also classified as a RAMSAR site, which highlights its significance as a wetland of international importance. Two other sites were located in Bourgneuf Bay, France (Figure 1 B : 46.9849°N, 2.1488°W) which is a 340 km² semi-enclosed macrotidal bay, protected from waves by Noirmoutier Island. Bourgneuf bay hosts a large intertidal seagrass meadow of about 6 km² [42]. Within this meadow, the sites observed by drones (L'Epine and Barbatre) contained monospecific beds of *Zostera noltei* (dwarf eelgrass) with very little mixing with other macrophytes. Bourgneuf Bay is also part of the Natura 2000 network and serves as a RAMSAR site due to its critical habitat for migratory bird species and its extensive seagrass meadows [4]. Three sites were surveyed in the Ria de Aveiro Coastal Lagoon in Portugal (Figure 1 C : 40.6887°N, 8.6810°W). The extent of this lagoon is ~83 km² (at low tide) with many narrow channels, large salt marshes and many mudflats that uncover at low tide [43]. It is connected to the open sea through a single channel, with a tidal lag between the North and the South of the lagoon. The southernmost site (Gafanha) is a mudflat located in the Mira channel (one of the four main channels of the lagoon) whereas the two other sites (Mataducos and Marinha

Lanzarote) were situated in the middle of the lagoon and only accessible by boat. These Portuguese sites are characterized by a more diverse intertidal vegetation, where patches of seagrass intermingle with red, brown, and green macroalgae. The Aveiro Lagoon, like the other study areas, is a Natura 2000 site and a RAMSAR wetland, recognized for its rich mosaic of habitats and importance for biodiversity, including migratory bird species and intertidal vegetation.

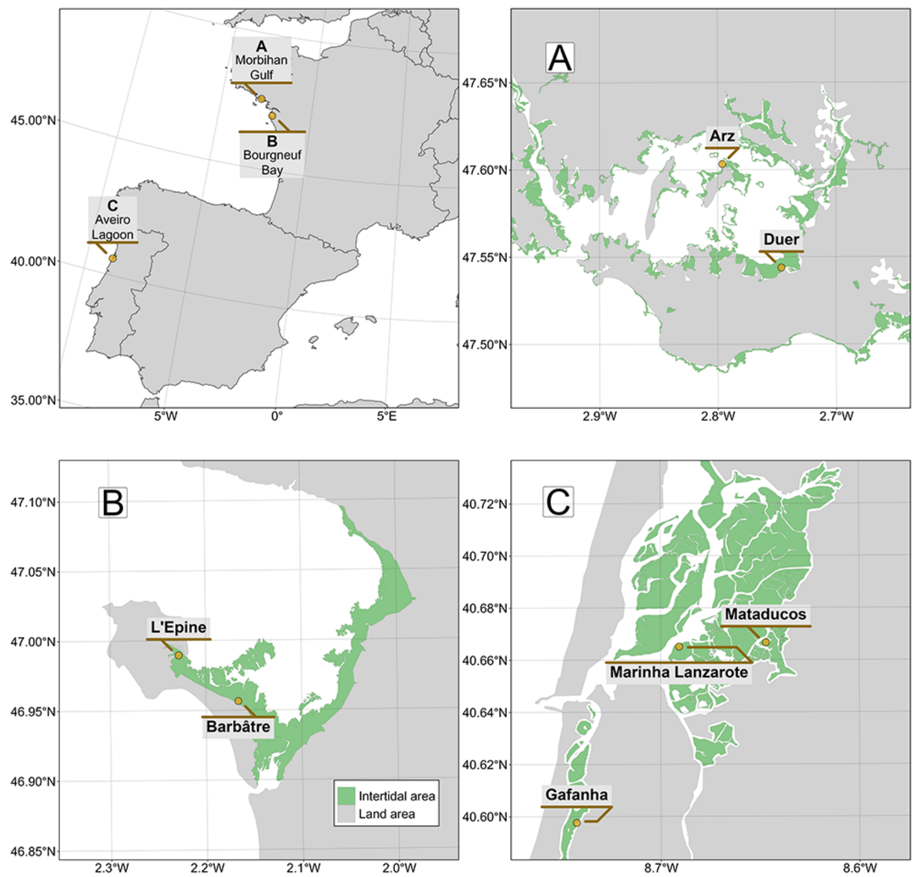

Figure 1: Location of drone flights in France and Portugal. A: Gulf of Morbihan (Two sites), B: Bourngeuf Bay (Two sites), C: Ria de Aveiro Coastal Lagoon (Three sites). Green areas represents the intertidal zone.

2.2. Field sampling

2.2.1. Drone acquisition

At each location, a DJI Matrice 200 quadcopter drone equipped with a Micasense RedEdge Dual MX multispectral camera was flown to take 1.2 million pixel reflectance photographs with ten spectral bands ranging from the blue to

Table 1: List of drone flight, summarising the date, the altitude, and the purpose of each flight. 12 m and 120 m flights have a spatial resolution of 8 and 80 mm respectively.

Country	Site	Name	Altitude	Utility	Date
France	Gulf of Morbihan	Arz Island	12m	Training	29/09/2022
		Duer	12m	Training	14/07/2022
		Duer	120m	Validation	14/07/2022
	Bourgneuf Bay	Barbâtre	120m	Validation	07/09/2021
		L'Epine	120m	Validation	08/07/2021
Portugal	Aveiro Lagoon	Marinha Lanzarote	120m	Validation	17/06/2022
		Mataducos	120m	Validation	16/06/2022
		Gafanha	120m	Validation	15/06/2022
		Gafanha	12m	Training	15/06/2022

the near infrared (NIR): 444, 475, 531, 560, 650, 668, 705, 717, 740 and 840 nm. To ensure consistent lighting conditions across flight paths, the drone's trajectory was aligned to maintain a solar azimuth angle of 90 degrees. An overlap of 70% and 80% (side and front respectively) between each image was set for each flight. A downwelling light sensor (DLS2) was used to acquire irradiance data concomitantly with the camera measurements. Raw data were calibrated in reflectance using a calibration panel reflective at ~50% provided by the manufacturer. Across all sites, flights were made at two different altitudes : 12 m or/and 120 m, with a spatial resolution of 8 mm and 80 mm, respectively (Table 1). **Low altitude flights were used as training dataset for a neural network model while high altitude flight were used for validation.**

2.2.2. Ground Control Points

Before each flight, targets used as ground control points were distributed over the study site and georeferenced with a Trimble © Geo XH 6000 differential GPS (dGPS). Ground control points were used to correct georeferencing imprecision of orthomosaics with an horizontal and vertical accuracy of 10cm. A dGPS was also used to georeference quadrats of 0.25 m^2 ,which assessed the presence or absence of five key taxonomic classes of intertidal vegetation : Bacillariophyceae (unicellular benthic diatoms forming biofilms at the sediment surface during low tide, **ranging in size from small patches (m^2) to entire mudflats (km^2)**; henceforth: Diatoms), Phaeophyceae (henceforth: brown macroalgae), Magnoliopsida (henceforth: Seagrasses), Chlorophyceae (henceforth: Green macroalgae) and Rhodophyceae (henceforth: red macroalgae) (Figure 2). Only homogeneous vegetation patches extending over several meters were selected as ground control points. Pictures of each quadrat were uploaded online to the open-portal Global Biodiversity Information Facility (GBIF) platform [44]. Each photograph was also processed to estimate the percent cover of each type of vegetation using an image processing software [ImageJ, 45]. Hyperspectral reflectance signatures of each vegetation class were recorded using an ASD FieldSpec HandHeld 2 spectroradiometer, which acquires reflectance between 325 and 1075 nm, with 1 nm of spectral resolution. Hyperspectral signatures served dual purposes: they validate the radiometric calibration of drone data and contribute to misclassification reduction in photo interpretations.

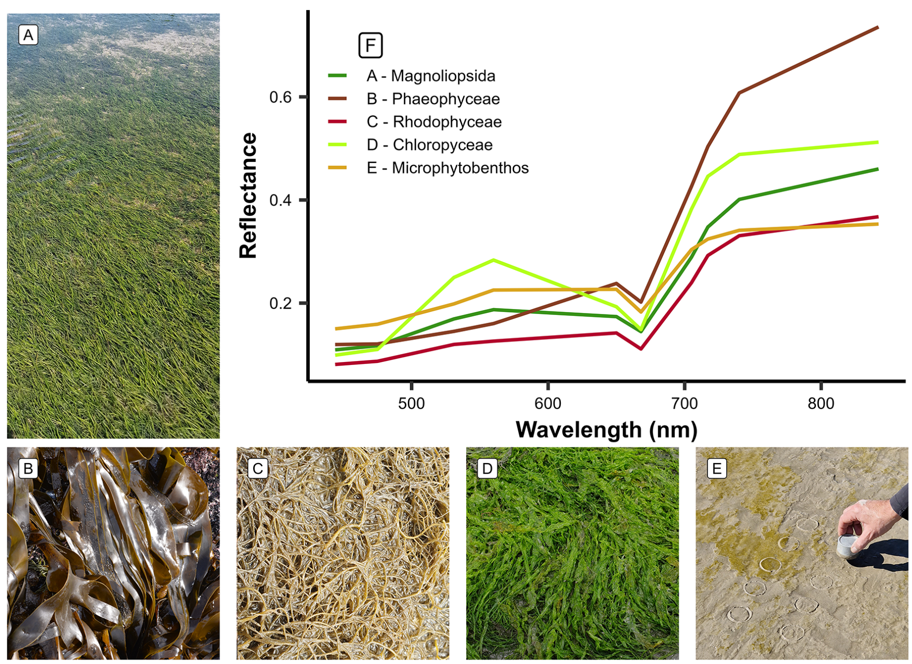

Figure 2: The five taxonomic classes of vegetation used to train the Neural Network model and an example of their raw spectral signatures at the spectral resolution of the Micasense RedEdge Dual MX. A : Magnoliopsida (*Zostera noltei*) ; B : Phaeophyceae (*Fucus sp.*) ; C : Rhodophyceae (*Gracilaria vermiculophylla*) ; D : Chlorophyceae (*Ulva sp.*) ; E : Bacillariophyceae (Diatoms - MPB). **Classes were identified following the World register of Marine species.**

2.3. Drone Processing

A structure-from-motion photogrammetry software [Agisoft Metashape, 46] was used to process images to obtain multispectral orthomosaics of each flight. The process for orthomosaicking was identical for every flight. First, key tying points were detected inside of each image and between overlapping images in order to obtain a sparse point cloud. This cloud was cleaned using a reprojection accuracy metric in order to remove noisy points. A dense point cloud was then produced using a structure from motion algorithm. A surface interpolation of this dense point cloud was made to obtain a digital surface model (DSM), used to reconstruct the multispectral ortho-image [47]. Low altitude drone flights produced ortho-images with a very high spatial resolution (8 mm per pixel), making it efficient to visually distinguish between the various types of vegetation. High altitude flights allowed to cover larger areas and produced images with a pixel size of 80 mm (Table 1).

2.4. General Workflow

The spectral similarities of the reflectance signatures at the spectral resolution of the micasense senor between intertidal green macrophytes (Magnoliopsida and Chlorophyceae) make their discrimination challenging using simple classification algorithms (Figure 2 F). To overcome this challenge, a deep learning classification method was trained, validated, and applied to each drone flight (Figure 3).

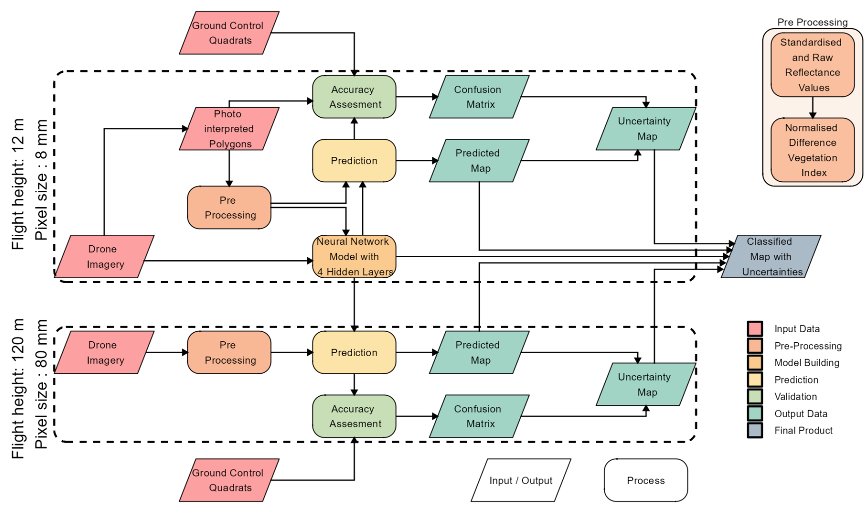

Figure 3: Schematic representation of the workflow. Parallelograms represent input or output data, and rectangles represent Python processing algorithms. The overall workflow of this study is divided into two distinct parts based on the spatial resolution of the drone flights: high-resolution flights (pixel size: 8 mm) were utilized for training and prediction of the Neural Network model, whereas lower-resolution flights (pixel size: 80 mm) were solely employed for prediction purposes. Validation has been performed on both high and low resolution flights.

2.4.1. Training dataset building

A dataset containing photo-interpreted drone reflectance pixels was built to train a Neural Network model. The training pixels were categorized into seven different classes, representing the various habitats encountered at the different study sites: Sediment, Water, green macroalgae, seagrasses, diatoms, brown

Table 2: Vegetation Classes of the model and the number of pixels used to train and validate each class

Name	Taxonomic Class	Training Pixels	Validation Pixels
Diatoms	Bacillariophyceae	4,475	9,807
Green macroalgae	Chlorophyceae	17,140	25,910
Seagrass	Magnoliopsida	221,065	179,119
Brown macroalgae	Phaeophyceae	169,936	82,161
Red macroalgae	Rhodophyceae	5,771	10,054
Water	-	83,677	76,612
Sediment	-	95,126	57,299

macroalgae and red macroalgae. Only data from the low-altitude flights (Table 1) were used for training because their 8 mm spatial resolution allowed to avoid spectral sub-pixel mixing and to accurately identify vegetation classes. **In the field, seagrasses displaying two distinct colors, each with a unique spectral signature, were observed. Careful attention was given to incorporating training pixels from both color types into the training dataset for the seagrass class. This approach was consistently applied to all classes within the model.** More than 418,000 pixels at 8 mm resolution from the 3 training flights were used to train the model (Table 2). Twenty one variables were used by the model as predictors: the ten raw spectral bands of the Micasense RedEdge Dual MX multispectral camera (ranging from 444 nm to 840 nm), the same ten spectral bands standardized using a min/max transformation (Equation 1 ; [48]) and the Normalized difference vegetation index (NDVI, Equation 2). Standardisation of spectral bands is commonly used to eliminate the scaling differences between spectra and to limit the effect of biomass on the spectra shape [26, 27].

$$R_i^*(\lambda) = \frac{R_i(\lambda) - min(R_i)}{max(R_i) - min(R_i)} \tag{1}$$

where $R_i(\lambda)$ is the reflectance at the wavelength (λ) of each individual spectra (i), $min(R_i)$, and $max(R_i)$ are the minimum and maximum value of the spectra (i)

$$NDVI = \frac{R(840nm) - R(668nm)}{R(840nm) + R(668nm)} \tag{2}$$

where $R(840nm)$ is the reflectance at 840 nm and $R(668nm)$ is the reflectance at 668 nm.

2.4.2. Model building

A neural network classification model was built using the fastai workflow [49]. This model was composed of 2 hidden layers and have a total of 26 054 trainable parameters. Parameters have been fine tuned using 12 epoch to minimize the error rate. This model has been called DISCOV, standing for Drone Intertidal Substrat Classification Of Vegetation.

2.4.3. Validation

The workflow of this study revolves around two distinct flight heights (12 and 120 m, Figure 3) where ensuring consistency between reflectances at both heights is crucial. This comparison was conducted at sites where low and high altitude flights overlapped. The low altitude flights were resampled to the same spatial resolution and grid as the high flights using a median resampling method. Reflectance values were then extracted, and a scatterplot was generated and the Root Mean Square Error (RMSE) was computed to compare the difference bewteen the raw and standardised reflectance.

The classification model was applied to all flights at both 12 and 120 m of altitude. *In situ* information on georeferenced class type and percent cover, acquired over homogeneous vegetation patches at the same time as drone flights was used to assess the model accuracy. These images were used to construct a validation dataset indicating the presence or absence of each class. Additionally to the quadrat-based validation dataset, polygons of each class were photo interpreted in order to increase the number of pixels of the validation dataset. A total of 536,000 pixels were used to validate the Neural Network classifier. The sites with the lowest and highest number of validation data were Gafanha Low (17316 pixels) and Marinha Lanzarote (159713 pixels), respectively. A confusion matrix, along with precision metrics such as global accuracy, sensitivity, specificity, F1 score, and Kappa coefficient, were generated for each site. These metrics were computed as follow :

$$\text{Global accuracy} = \frac{\sum_{i=1}^{k} \mathrm{TP}_i}{\sum_{i=1}^{k} (\mathrm{TP}_i + \mathrm{FP}_i + \mathrm{FN}_i)}$$

$$\text{Sensitivity}_i = \frac{\mathrm{TP}_i}{\mathrm{TP}_i + \mathrm{FN}_i}$$

$$\text{Specificity}_i = \frac{\mathrm{TN}_i}{\mathrm{TN}_i + \mathrm{FP}_i}$$

$$\mathrm{F1}_i = \frac{2 \cdot \mathrm{TP}_i}{2 \cdot \mathrm{TP}_i + \mathrm{FP}_i + \mathrm{FN}_i}$$

Where TP_i, TN_i, FN_i and FP_i represent the true positives, true negatives, false negatives and false positives relative to the class i.

All validation matrices were then aggregated to create an overall matrix

2.5. Variable Importance

Variable Importance Plots (VIP) serve as a method to identify which predictors are important for predicting a specific class. Out of the 21 predictors utilized in this study, Variable Importance was computed only for the raw and standardized values of the 10 spectral bands captured by the MicaSense camera. This is achieved by repeatedly predicting the same dataset while randomly shuffling one predictor at a time. The benchmark score obtained after each iteration is then compared to the benchmark score obtained without shuffling any variables. The greater the difference between these two benchmark values, the more important the variable is for the model [50].

2.6. Influence of the spatial resolution on classification

To assess the impact of spatial resolution on the model's output, we resampled the drone orthomosaics from their native resolution (8 cm for high-altitude flights) using the "average" method from the terra package in R. **The rasters were resampled to 32 different resolutions, ranging from 10 cm to 30 m.** DISCOV was then applied to these resampled rasters, and the results were compared to the original model predictions. For each resolution and vegetation class, we calculated the predicted area loss, where a score of 0 indicates no area loss during spatial resampling, and a score of 100 indicates complete loss of the vegetation class.

We used a Generalized Linear Model (GLM) with a Beta distribution to examine the relationship between pixel resolution, vegetation class, and their interaction on the loss of vegetation. The loss of vegetation was modelled as function of the interaction between pixel resolution and vegetation class (Diatoms, brown macroalgae, seagrass, green macroalgae and red macroalage). Sample vs fitted residuals and quartile-quartile graphics were assessed visually, to ensure assumption of the models used were met.

2.7. Impact of mixed vegetation cover on the prediction

The key aspect of the workflow adopted in the present study is the mapping at two different altitudes (12 and 120 m), resulting in two distinct resolutions for the same area (8 and 80 mm; respectively). The high-resolution flight was used to estimate the sub-pixel composition for each pixel of the lower-resolution flight. Consequently, within each pixel of the high-altitude flights, the contribution of each vegetation class (% cover) was obtained, and a kernel density plot was generated. This plot provided a visual representation of the model's behavior in mixed vegetation scenarios. It helps to understand the minimum vegetation cover of a given class within a pixel necessary for the model to confidently predict that class.

3. Results

3.1. Reflectance comparison between the two different altitudes

In this study, drone flights were conducted at two different altitudes (12 and 120 m) to construct the neural network model. At the sites where the flights at both altitudes overlapped, reflectance was compared. Overall there was a good agreement between the two altitudes (RMSE : 0.027 ; Figure 4).

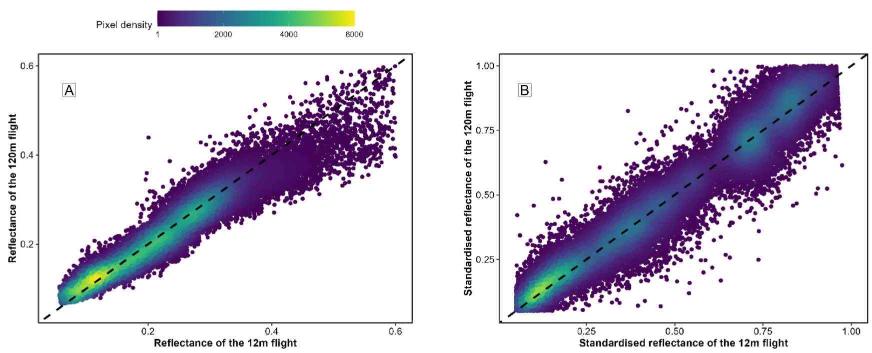

Figure 4: Comparison of reflectance retrieved from both low-altitude and high-altitude flights over a common area. The black dashed line represents a 1 to 1 relationship. Left (A) plots raw data and right (B) plots standardized data (Equation 1).

There was a slight underestimation for raw reflectance values in the high-altitude flight, particularly for higher reflectance values (Figure 4 A). Since both flights were conducted over vegetated areas, the highest reflectance values correspond to the infrared part of the spectrum. This difference was not present when the reflectance has been standardized (Equation 1 ; Figure 4 B).

3.2. Classification

Each drone flight was used to produce a prediction map, as well as a probability map that indicates the model derived probability of the selected class for every pixel. The low-altitude flight conducted in Gafanha, Portugal, represented the site with the highest complexity (Figure 5). Among the five vegetation classes on which the model was trained, four were present on this site, with green and red macroalgae mixed with a seagrass meadow. There was also diatoms forming biofilms on bare sediment surface. Although the seagrass was solely composed of a single specie, *Zostera noltei*, various colors of this specie could be observed from dark green (corresponding to healthy leaves) to brown (when leaves are senescent or have an altered pigment composition). Regardless of the variation of color, the class Magnoliopsida (seagrass) was accurately predicted by the model (F1 score of 0.96 at that site).

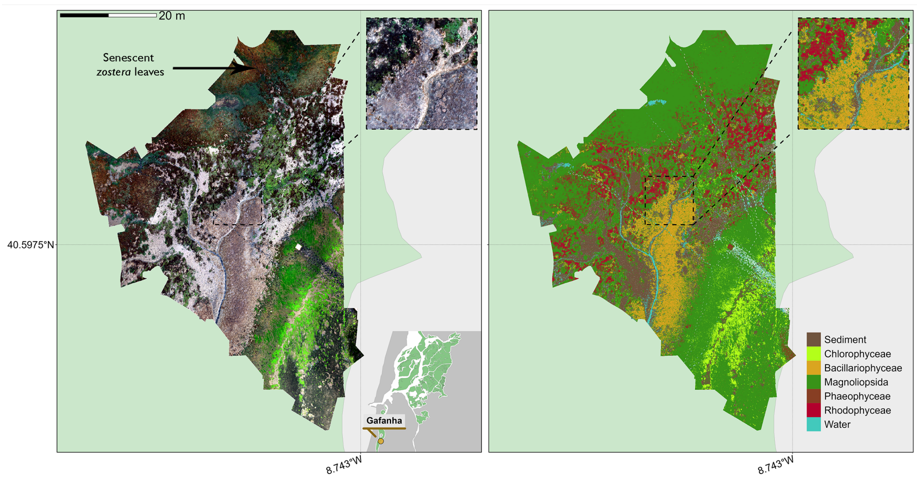

Figure 5: RGB orthomosaic (Left) and Prediction (Right) of the low altitude flight of Gafanha, Portugal. The total extent of this flight was 3000 m² with a resolution of 8 mm per pixel. Background colors indicate intertidal area (Light Green) and land area (Light Grey). The zoom covers an area equivalent to a 10-meter Sentinel-2 pixel size.

The high-altitude flight over Gafanha covered a total area of ~1 km² (Figure 6). A channel contouring a small island was masked in the prediction map. Most of vegetation area was classified as seagrass by the model, including patches with discolored leaves. Only a few pixels were classified as green macroalgae (F1 score of 0.55). Patches of red macroalgae were correctly classified (F1 score of 0.85). In the northern part of the site and near the land eadges, patches of the schorre angiosperm *Sporobolus maritimus* (syn. *Spartina maritima)* were misclassified, either as seagrass or as brown algae (F1 score of 0.77 and 0.71, respectively).

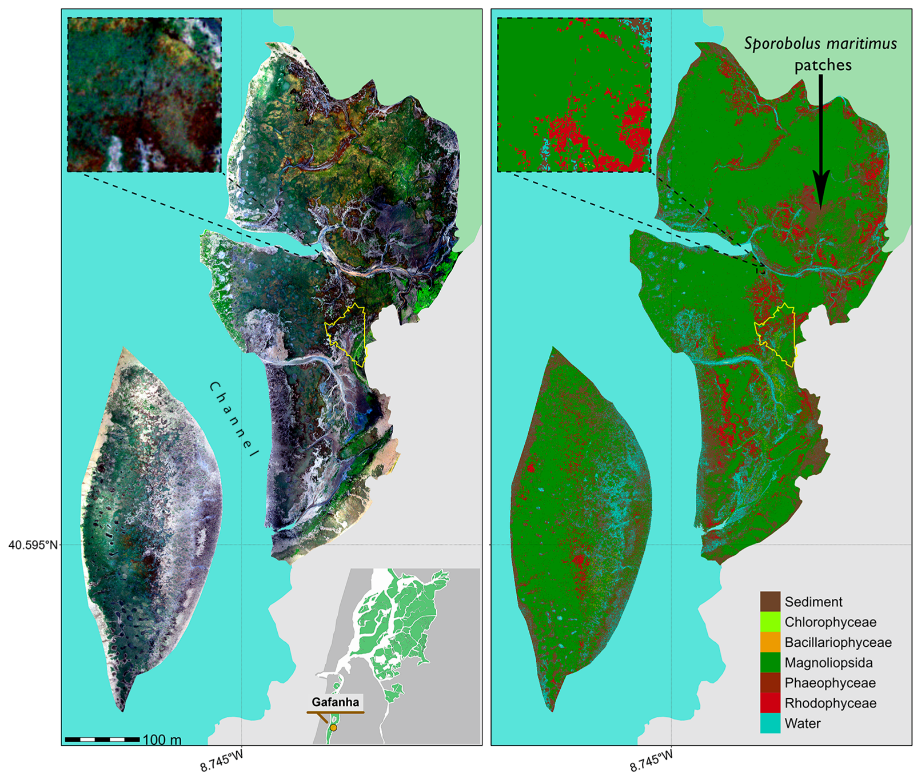

Figure 6: RGB orthomosaic (Left) and Prediction (Right) of the high altitude flight of Gafanha, Portugal. The total extent of this flight was about 1 km² with a resolution of 80 mm per pixel. Background colors indicate intertidal area (Light Green), land area (Light Grey) and water (Light Blue). The yellow outline shows the extent of the low altitude flight of Gafanha presented in Figure 5. The zoom covers an area equivalent to a 10-meter Sentinel-2 pixel size.

Among the high altitude flights, the one acquired over the inner part of Ria de Aveiro coastal lagoon covered the largest area with approximately 1.5 km² (Figure 7). Teh vegetation present at the site was dominated by seagrass and red macroalgae. The classification provided consistent results, with a patchy seagrass meadow mixed with red macroalgae on the eastern part of the site. As shown in the zoom (Figure 7), the edges of the meadow were mixed with green macroalgae (*Ulva sp.*), which the model agreed with (F1 score of 0.89 for green algae, 0.97 for seagrass and 0.98 for red algae).

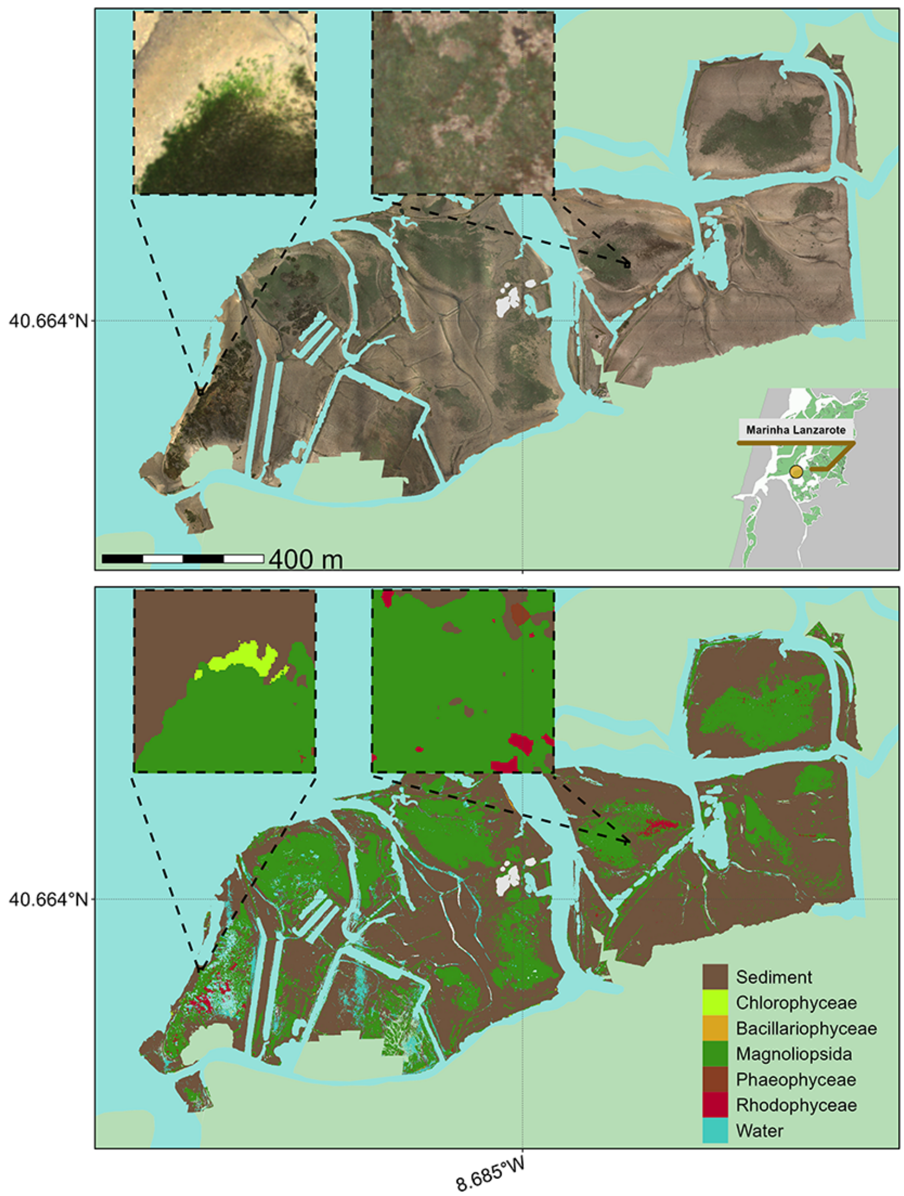

Figure 7: RGB orthomosaic (Top) and Prediction (Bottom) of the flight made in the inner part of Ria de Aveiro Lagoon, Portugal. The total extent of this flight was about 1.5 km² with a resolution of 80 mm per pixel. Background colors indicate intertidal area (Light Green), land area (Light Grey) and water (Light Blue). The zoom inserts cover an area equivalent to the size of a 10-meter Sentinel-2 pixel.

The flight over L'Epine in Noirmoutier Island, France (Figure 8 A) was conducted near a dike, which crossed the northern part of the site from West to East. Alongside this dike, Fucale brown macroalgae (*Fucus spp.*, *Ascophyllum nodosum*) were attached to sparse rocks, and stranded green algae (*Ulva spp.*) could be observed, which was correctly reproduced by the prediction (Figure 8 B). This site was characterized by a high mixture between green macroalgae and seagrass but these two classes were correctly discriminated by the classifier (F1 score of 0.97 and 0.98 respectively).

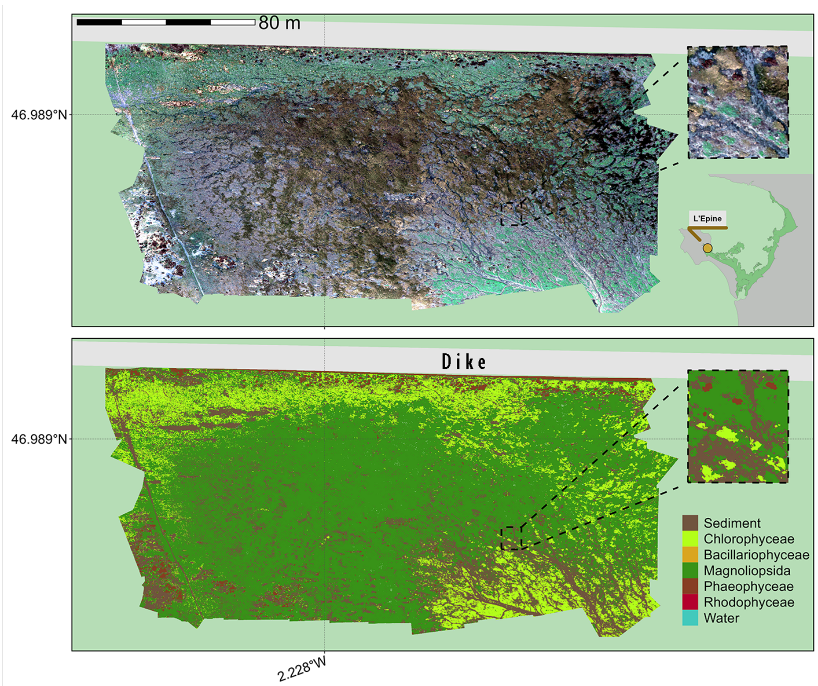

Figure 8: RGB orthomosaic (Top) and Prediction (Bottom) of L'Epine, France. The total extent of this flight was about 28 000 m² with a resolution of 80 mm per pixel. Background colors indicate intertidal area (Light Green) and land area (Light Grey). The zoom covers an area equivalent to a 10-meter Sentinel-2 pixel size.

3.3. Validation of the model

With all drone flights combined, the model global accuracy was 94.26% with a Kappa coefficient of 0.92 (Figure 9).

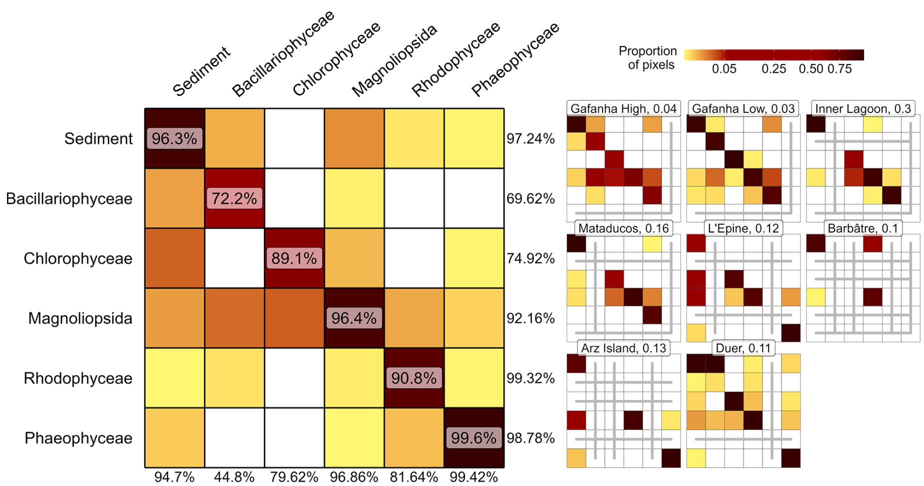

Metrics	Sediment	Bacillariophyceae	Chlorophyceae	Magnoliopsida	Rhodophyceae	Phaeophyceae	Overall
Sensitivity	0.95	0.45	0.8	0.97	0.82	0.99	0.83
Specificity	0.98	1	0.99	0.96	1	1	0.99
Accuracy	0.96	0.72	0.89	0.96	0.91	1	0.94

Figure 9: A global confusion matrix on the left is derived from validation data across each flight, while a mosaic of confusion matrices from individual flights is presented on the right. The labels inside the matrices indicate the balanced accuracy for each class. The labels at the bottom of the global matrix indicate the User's accuracy for each class, and those on the right indicate the Producer's Accuracy. The values adjacent to the names of each site represent the proportion of total pixels from that site contributing to the overall matrix. Grey lines within the mosaic indicate the absence of validation data for the class at that site. The table at the bottom summarizes the Sensitivity, Specificity, and Accuracy for each class and for the overall model.

The lowest performing site was Gafanha High (global accuracy of 75.45%) whereas Mataducos was the site with the most accurate prediction (global accuracy of 98.05%). Overall, the classes Phaeophyceae, Magnoliopsida, Sediment and Rhodophyceae were correctly classified with a balanced accuracy of 1, 0.96, 0.96 and 0.91 respectively. Bacillariophyceae was the least accurate class (accuracy of 0.72) mainly due to confusion with Magnoliopsida and Sediment.

3.4. Variable importance

The computation of the variable importance made it possible to identify which bands were the most useful for class prediction (Figure 10).

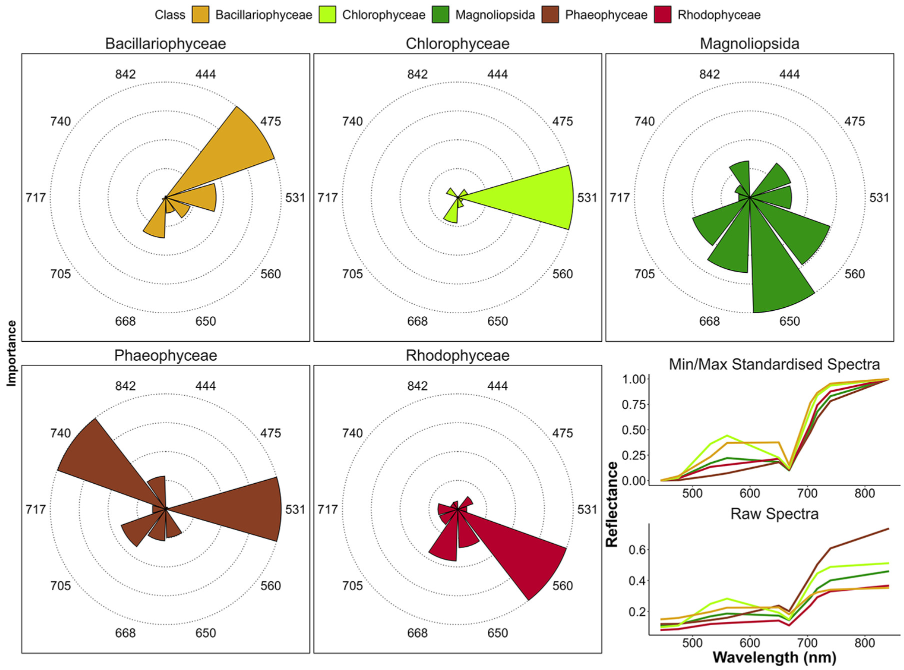

Figure 10: Variable Importance of the Neural Network Classifier for each taxonomic class. The longer the slice, the more important the variable for prediction of each class. The right plot shows the drone raw and standardised reflectance spectra of each class. Each slice represents the Variable Importance (VI) of both raw and standardised reflectance combined.

The spectral bands at 444, 717 and 842 nm of the Micasense camera did not provide important information to discriminate any of the vegetation classes. The band at 531 nm was the most important predictor by far for the classifier to accurately predict Chlorophyceae. In fact, at this wavelength, the Chlorophyceae spectra showed the highest reflectance among all vegetation classes (Figure 2 F). The bands at 531 and 740 nm were the most important predictors for Phaeophyceae, corresponding to the lowest reflectance among all classes. Bands at 475 and 560 nm were the most important predictors for Bacillariophyceae and Rhodophyceae, respectively. Four predictors, ranging from the green (560 nm) to the RedEdge (705 nm) bands were important to accurately predict Magnoliopsida.

3.5. Effect of spatial resolution on the classification

Clear differences were seen in vegetation loss across different resolutions and vegetation classes (Figure 11). At a fine resolution of 1m, changes in the retrieved area for each vegetation type are minimal. Green algae shows the highest loss, with 1.2% area lost compared to the native resolution (80 mm). As the resolution coarsens to 10m, vegetation loss becomes more pronounced, with green macroalgae again experiencing the greatest reduction (12% compared to

8cm) and seagrass showing the smallest loss (1.3%). At a resolution of 30m, all green algae have been lost (100% compared to 8cm), while seagrass experiences a relatively small reduction of 11%. Brown macroalgae and red macroalgae show moderate declines, with losses at 30m resolution reaching approximately 37% and 59%, respectively.

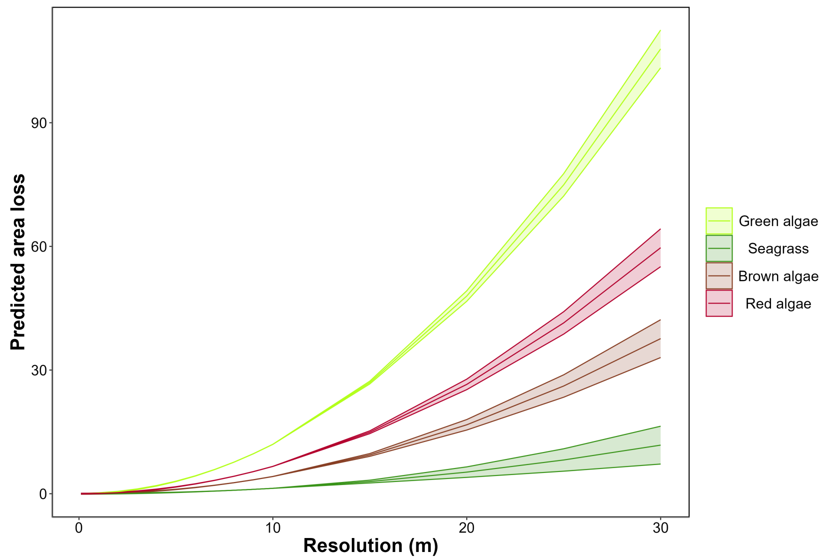

Figure 11: Predicted area loss for different vegetation types (green algae, seagrass, brown algae, red algae) as a function of spatial resolution. Lines represent Generalized Linear Model (GLM) predictions, and shaded areas indicate standard errors. As resolution decreases, predicted area loss increases for all vegetation types, with green algae showing the highest loss and seagrass the smallest at coarser resolutions.

3.6. Effect of the percent cover on the prediction

Using the very high resolution low altitude flight (8 mm pixels), we determined the minimal percent cover required to correctly classify a given class within the corresponding high altitude flight (8cm pixel resolution ; Figure 12).

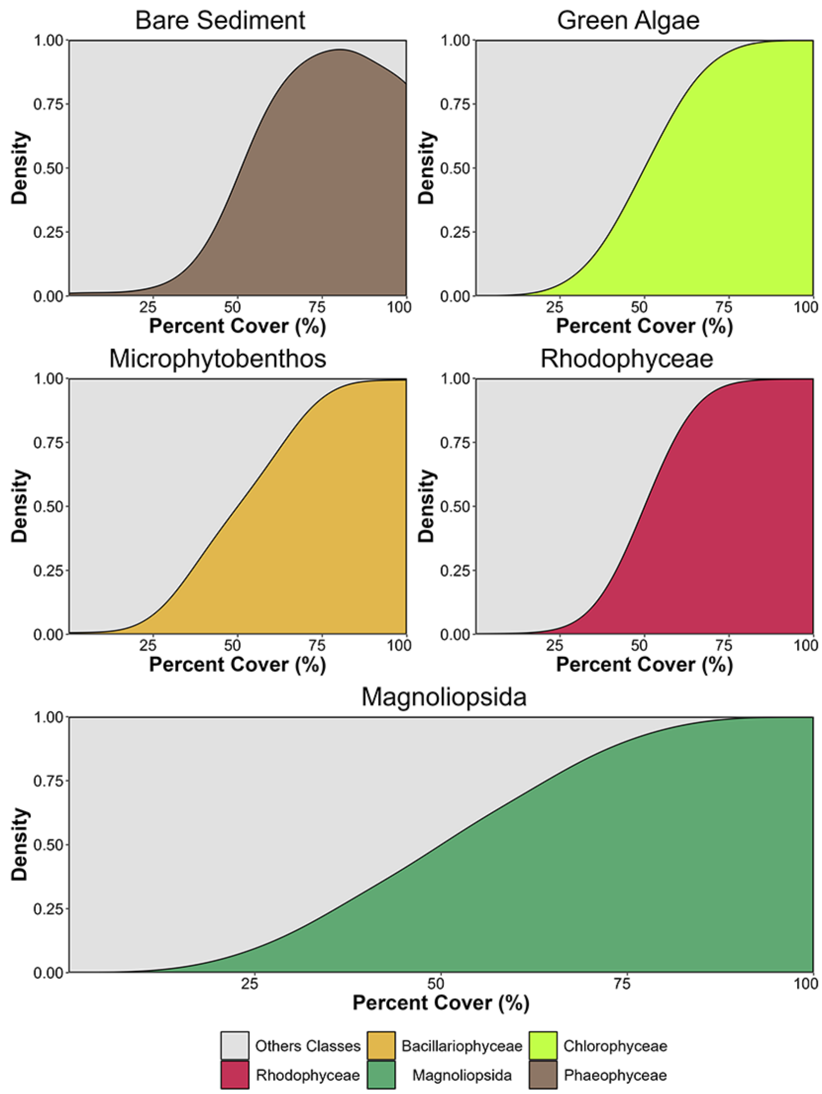

Figure 12: Kernel density plot showing the proportion of pixel well classified based on the percent cover of the class in high altitude flight pixels of Gafanha, Portugal. Each subplot shows all the pixels of the same classes on the high altitude flight. Percent cover of classes was retrieved using the result of the classification of the low altitude flight of Gafanha, Portugal.

A percent cover of at least 80% was sufficient to have all the 80 mm pixels correctly classified, with the exception of Magnoliopsida that required a higher cover (>90 %) to be accurately classified. Concerning the probability of each class, there is a linear relationship between the percent cover and the confidence of the model to predict the class. To predict green macroalgae with a model likelihood of 0.85, a cover of 93 % was needed, 90 % for seagrass, 92 % for red macroalgae and 97 % for diatoms When the vegetation cover of a given class was 100 %, coarser high-flight pixels were correctly classified for all the classes except for Bare Sediment, which was only correctly classified 80% of the time. This phenomenon may be attributed to the time gap between the two flights, allowing for microphytobenthos migration to the sediment surface during low tide, consequently altering the model's classification from bare sediment to Bacillariophyceae.

4. Discussion

4.1. Vegetation Discrimination

The primary objective of this study was to develop a method for the accurate classification of emerged macrophytes observed during low tide on tidal flats, specifically focusing on distinguishing between Chlorophyceae (green macroalgae) and marine Magnoliopsida (seagrasses) using a multispectral resolution. The discrimination between seagrasses and green macroalgae is challenging due to their optical similarity in the visible range [51, 28, 52]. These two macrophytes share a similar pigment composition: chlorophyll-a (common to all vegetation types), chlorophyll-b (an additional photosynthetic pigment), and accessory carotenoids such as zeaxanthin, lutein and neoxanthin (Figure 13). Their spectral responses could be close, particularly at a multispectral resolution. Seagrass and green macroalgae frequently co-occur in intertidal areas, and can intermingle within a remote sensing pixel if the spatial resolution is too low. Here, the issue of intra-pixel mixing was resolved thanks to the very high spatial resolution of the drone (from 8 to 80 mm). In this study the risk of spectral confusion was avoided with a machine-learning approach exploiting a neural networks classifier. Our drone flights and a recent study based on *in situ* radiometry, suggested that a sensor with at least eight spectral bands ranging from 500 to 850 nm, and including a green band at 530 nm and a RedEdge band at 730 nm, was crucial to accurately discriminate green macroalgae from seagrasses [27].

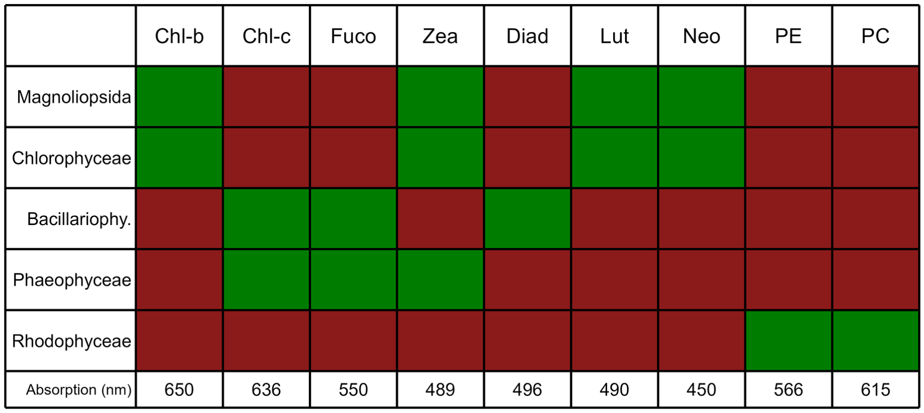

Figure 13: Photosynthetic and carotenoid pigments present (Green) or absent (Red) in each taxonomic class present in the Neural Network Classifier, along with their absorption wavelength measured with spectroradiometer, Chl-b: chlorophyll-b, Chl-c: chlorophyll-c, Fuco: fucoxanthin, Zea: zeaxanthin, Diad: diadinoxanthin, Lut: lutein, Neo: neoxanthin, PE: phycoerythrin, PC: phycocyanin [25; 26, [53]; 54; 55].

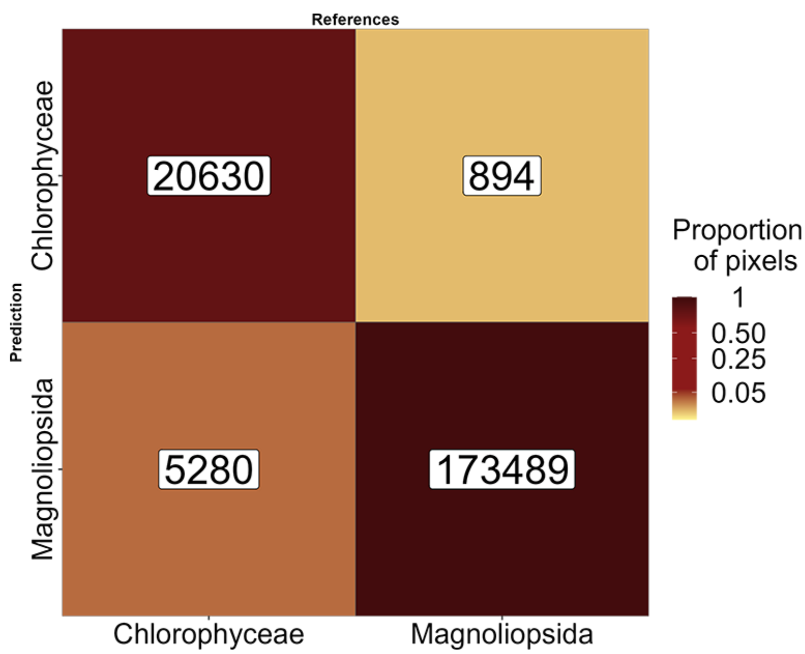

Figure 14: Sample of Figure 9 focusing on green macrophytes. The labels inside the matrix indicate the number of pixels.

Meeting these two criteria, the Micasense RedEdge-MX DUAL camera used in this study, enabled the classifier to achieve 97% of accuracy between these two classes (Figure 14). Even if their pigment composition is similar, differences in the spectral shape can be observed, with green algae having a higher reflectance peak at 560 nm as well as a higher NIR plateau than seagrass (Figure 2). Such differences were previously attributed to differences in pigments concentration and/or ratios [56], cellular structure as well as in the orientation of the plant at the sediment surface [57, 58, 59].

The variable importance analysis (Figure 10) identified that the band at 531 nm was the most important for accurately identifying Chlorophyceae. In fact, at this wavelength, Chlorophyceae exhibited the highest reflectance among all other classes, highlighting the difference in carotenoid to chlorophyll-a ratios between seagrasses and green macroalgae [60]. Concerning Phaeophyceae, the thick cell walls of these macroalgae [61] make it more reflective in the infrared part of the spectra [62], while the presence of fucoxanthin and zeaxanthin result in a low reflectance in the visible region (Figure 10 ; Figure 13). These two key features have been identified by the Neural Network as the two principal predictors to accurately identify brown algae (Figure 10). Similarly, the presence of phycoerythrin and phycocyanin in Rhodophyceae contribute to the lowest reflectance among all classes in the spectral range from 560 to 615 nm (Figure 10). Indeed the band at 560 nm has been identified as important for identifying this class, likely due to phycoerythrin absorption at this wavelength. Regarding Bacillariophyceae, 475 nm was the most important predictor for this class (Figure 10). Indeed, the reflectance at 475 nm was higher for Bacillariophyceae than for any other vegetation class (Figure 2), very likely due to the low biomass (and associated concentration of blue-absorbing pigments) of these unicellular organisms compared to seagrass and macroalgae.

4.2. Altitude and Temporal Effects on Vegetation Prediction Accuracy

The ability to differentiate between various types of vegetation plays a critical role in ecological monitoring and coastal management [63]. By distinguishing between seagrasses and macroalgae, our approach facilitates targeted conservation strategies, enabling more effective preservation and restoration efforts in coastal ecosystems. While comparing the reflectance at two different altitudes (12 m and 120 m with a spatial resolution of 8 and 80 mm, respectively), a nearly one-to-one relationship was observed, with a Root Mean Square Error (RMSE) of 0.02 (Figure 4). This result indicates that the reflectance measured by remote sensing (RS) sensors is not significantly influenced by pixel size. This finding is valuable for integrating drone-based data into larger-scale mapping projects (e.g., combining satellite and drone mapping in side-by-side analyses). The consistency of reflectance across altitudes suggests that drones can be effectively used for finer-scale mapping without compromising data accuracy when merging with other platforms. However, it was observed that there is an underestimation of the infrared part of the spectra in the high-altitude dataset (Figure 4). Such disparity in infrared reflectance may stem from temporal differences between the flights, possibly resulting in a slightly drier intertidal area and consequently higher infrared reflectance. This disparity poses an issue for the methodology followed in the present study, relying solely on one flight height for training. To address this issue, we employed min/max standardized reflectance spectra as predictors for the model Equation 1. This approach allowed us to eliminate the slight reflectance difference between the flights (Figure 4 B) and to focus on the shape of the spectra in the visible part of the electromagnetic spectra, where different pigmentation are associated to taxonomic diagnostic features. In contrast to subtidal seagrasses, which maintain a relatively constant biomass throughout the year, intertidal seagrasses, like the one studied in this work, exhibit strong seasonal phenology [24]. At some sites, they completely disappear during the winter and reach their peak above-ground biomass in the summer and early autumn. Along with these seasonal changes in biomass, the pigment composition and ratios also vary throughout the year, reflecting the plants' adaptations to different environmental conditions [56, 64]. Standardization of spectral signatures helps to mitigate the impact of changing biomass on the spectral profile, enabling the development of a model that can reliably predict vegetation across different geographical locations and seasons. This approach allows for consistent classification of vegetation despite variations in biomass and fluctuations in light conditions, providing a robust tool for monitoring and predicting vegetation dynamics [65, 66, 67]. We found 90 % seagrass cover was necessary at an 8 cm resolution for confident prediction of its presence (Figure 12). However, due to the strong phenology of intertidal seagrass meadows in Europe, the period when a meadow is well-established can be temporally restricted, limiting the ideal window for accurate detection.

4.3. Impact of Pixel Resolution on the prediction and Implications for Satellite Remote Sensing

Pixel resolution plays a critical role in accurately retrieving vegetation area from remote sensing data. As pixel size increases, we found a consistent decline in area retrieval is observed across all vegetation types, with more pronounced effects for certain types, such as green algae (Figure 11). This highlights the sensitivity of spatial resolution in detecting smaller or more fragmented vegetation features. Green algae, being particularly patchy across all study sites, shows the steepest decline in areal agreement as pixel size increases, which aligns with expectations given the limitations of coarser resolution in capturing fine-scale details.

This resolution-area relationship has important implications for satellite missions like Sentinel-2 and Landsat, which are commonly used in marine and coastal vegetation studies. Both satellites offer high-resolution imagery, with pixel sizes of 10m and 30m, respectively. While these resolutions are suitable for broad-scale environmental monitoring, they may be too coarse to capture finer-scale heterogeneity, particularly in fragmented vegetation like green algae. Our findings suggest that, while the 30m resolution of Landsat may be adequate for homogeneous vegetation types, such as seagrass, a higher resolution is essential for accurately mapping patchy vegetation like green algae. These findings have direct implications for environmental management and conservation planning. Overlooking fine-scale vegetation features, such as those seen in green algae, could result in inadequate protection or restoration efforts, particularly in ecologically sensitive coastal zones, as early stages of green tides could be challenging to monitor at coarse resolutions.

Very high-resolution imagery offers more accurate vegetation mapping but comes with trade-offs. As resolution increases, data costs rise, and processing becomes more resource-intensive due to the larger file sizes and computational demands. Consequently, high-resolution data requires more storage and can slow down real-time applications. For large-scale monitoring of homogeneous vegetation types, 10 m resolution of S2/MSI or even the 30 m of Landsat/OLI are often sufficient. However, when mapping fragmented vegetation like green algae, the precision provided by higher-resolution imagery is crucial, despite the additional costs and processing challenges it imposes.

4.4. Towards climate and biodiversity applications

Climate change, global warming, eutrophication, alien and invasive species development, coastal erosion, and sea level rise are expected to continue impacting coastal ecosystems in the future [68, 69, 70] and the demand for meaningful and efficient monitoring of coastal habitats has never been higher[71, 72, 51]. Our findings, particularly the improved discrimination of intertidal seagrass and green macroalgae from other intertidal vegetation classes, highlight the potential of drone-based remote sensing to support diverse applications, from conservation of biodiversity to climate change adaptation strategies.

Due to increasing coastal eutrophication, macroalgal blooms are becoming increasingly common in many regions around the world [73, 74]. These blooms can have negative impacts on human health and local economic activities, including human health, fishing and aquaculture, tourism, and recreational activities [75, 74]. The first green tide events (i.e. bloom of green macroalgae of the genus *Ulva*) were reported in Brittany, France, in the 1970s and have since been a concern for local stakeholders and economic activities [76]. Some regions of the world have witnessed an increase in brown macroalgae blooms, predominantly involving algae of the genus *Sargassum* washing along the Caribbean coastlines [77], and more recently *Rugulopteryx okamurea* in southern Europe [37]. Satellite remote sensing has proven to be a valuable tool for mapping the spatial and temporal extent of macroalgal blooms worldwide. However, due to limitations in spatial resolution, it can only effectively map well-developed blooms [78, 79, 80]. High spatial resolution drone imagery, coupled with accurate classification algorithm, could be used to map the early stages of macroalgal blooms in areas known to have regular blooms or in new sites. Indeed, this approach could provide early warning alerts to local managers and complimentary to traditional sampling methods to monitor coastal ecosystems. These methods are generally time and resource-intensive, and the findings are often difficult to scale-up when applied alone. Earth Observation can bridge this gap and meet the needs for systematic monitoring of coastal ecosystems over large areas [81]. The retrieval of Essential Biodiversity Variables and Essential Ocean Variables through satellite observations has been increasingly common, enabling comprehensive monitoring of entire ecosystems over extended time periods [82, 14]. The Water Framework Directive [63] mandates the achievement and maintenance of "good ecological status" for all European waters, which necessitates a comprehensive understanding and monitoring of aquatic ecosystems, including coastal habitats like seagrass beds [83, 84, 14].

Effective and efficient monitoring tools are essential for identifying the impacts of human activities and natural changes on coastal ecosystems. On-demand, multispectral drone observations at very high spatial-resolution provide a novel and powerful tool to rapidly and accurately acquire ground truth data which can be used to develop machine-learning algorithm for satellite sensors [23]. Spatially resolved data are indeed critical for calibrating and validating satellite remote sensing observations, thereby enhancing our capacity to monitor vast coastal areas. The integration of drone technology facilitates a scalable approach to environmental surveillance while taking into account patchiness of secondary vegetation, offering significant advancements in the spatial and temporal resolution of data collection. This, in turn, supports the EU WFD's objectives by enabling more informed and timely management decisions for the conservation and restoration of aquatic ecosystems.

5. Conclusion

The utilization of very high spatial resolution (from 8 to 80 mm) drone-based remote sensing coupled with machine learning techniques has proven to be an effective method for the discrimination of intertidal seagrasses from green macroalgae with a multispectral resolution sensor. Standardized reflectance was incorporated in the Neural Network model allowing for a better discrimination of spectral features related to pigment absorption in the visible region of the spectrum. There was a striking difference between the variable of importance to discriminate Magnoliopsida from Chlorophyceae. The latter was essentially identified with the 451 nm spectral band while more spectral bands were needed to identify the former, notably 650, 560, 668, and 705 nm. As the spectral bands of the Micasense RedEdge Dual MX are very similar to those of Sentinel-2/MSI, we suggest that multispectral satellite data have the potential to perform this discrimination between these green macrophytes. The findings underscore the importance of adopting advanced remote sensing tools in ecological studies and environmental monitoring, providing a foundation for future research and policy implementation aimed at ecosystem conservation and restoration.

References

[1] R. K. Unsworth, L. C. Cullen-Unsworth, B. L. Jones, R. J. Lilley, The planetary role of seagrass conservation, Science 377 (6606) (2022) 609–613.

[2] A. I. Sousa, J. F. da Silva, A. Azevedo, A. I. Lillebø, Blue carbon stock in zostera noltei meadows at ria de aveiro coastal lagoon (portugal) over a decade, Scientific reports 9 (1) (2019) 14387.

[3] R. C. Gardner, C. Finlayson, Global wetland outlook: state of the world's wetlands and their services to people, Stetson Law, 2018.

[4] M. L. Zoffoli, P. Gernez, S. Oiry, L. Godet, S. Dalloyau, B. F. R. Davies, L. Barillé, Remote sensing in seagrass ecology: coupled dynamics between migratory herbivorous birds and intertidal meadows observed by satellite during four decades, Remote Sensing in Ecology and Conservation (12 2022). doi:10.1002/rse2.319.

[5] E. Jankowska, L. N. Michel, G. Lepoint, M. Włodarska-Kowalczuk, Stabilizing effects of seagrass meadows on coastal water benthic food webs, Journal of Experimental Marine Biology and Ecology 510 (2019) 54–63.

[6] H. M. Nguyen, P. J. Ralph, L. Marín-Guirao, M. Pernice, G. Procaccini, Seagrasses in an era of ocean warming: a review, Biological Reviews 96 (5) (2021) 2009–2030.

[7] L. M. Soissons, E. P. Haanstra, M. M. Van Katwijk, R. Asmus, I. Auby, L. Barillé, F. G. Brun, P. G. Cardoso, N. Desroy, J. Fournier, et al., Latitudinal patterns in european seagrass carbon reserves: influence of seasonal fluctuations versus short-term stress and disturbance events, Frontiers in Plant Science 9 (2018) 88.

[8] R. J. Orth, T. J. Carruthers, W. C. Dennison, C. M. Duarte, J. W. Fourqurean, K. L. Heck, A. R. Hughes, G. A. Kendrick, W. J. Kenworthy, S. Olyarnik, et al., A global crisis for seagrass ecosystems, Bioscience 56 (12) (2006) 987–996.

[9] H. Lin, T. Sun, Y. Zhou, R. Gu, X. Zhang, W. Yang, Which genes in a typical intertidal seagrass (zostera japonica) indicate copper-, lead-, and cadmium pollution?, Frontiers in Plant Science 9 (2018) 1545.

[10] J. E. Duffy, L. Benedetti-Cecchi, J. Trinanes, F. E. Muller-Karger, R. Ambo-Rappe, C. Boström, A. H. Buschmann, J. Byrnes, R. G. Coles, J. Creed, et al., Toward a coordinated global observing system for seagrasses and marine macroalgae, Frontiers in Marine Science 6 (2019) 317.

[11] M. A. Rasheed, R. K. Unsworth, Long-term climate-associated dynamics of a tropical seagrass meadow: implications for the future, Marine Ecology Progress Series 422 (2011) 93–103.

[12] R. M. Chefaoui, C. M. Duarte, E. A. Serrão, Dramatic loss of seagrass habitat under projected climate change in the mediterranean sea, Global change biology 24 (10) (2018) 4919–4928.

[13] C. B. de Los Santos, D. Krause-Jensen, T. Alcoverro, N. Marbà, C. M. Duarte, M. M. Van Katwijk, M. Pérez, J. Romero, J. L. Sánchez-Lizaso, G. Roca, et al., Recent trend reversal for declining european seagrass meadows, Nature communications 10 (1) (2019) 3356.

[14] M. L. Zoffoli, P. Gernez, L. Godet, S. Peters, S. Oiry, L. Barillé, Decadal increase in the ecological status of a north-atlantic intertidal seagrass meadow observed with multi-mission satellite time-series, Ecological Indicators 130 (2021) 108033. doi:10.1016/j.ecolind.2021.108033.
URL https://linkinghub.elsevier.com/retrieve/pii/S1470160X21006981

[15] M. Devlin, J. Brodie, Nutrients and eutrophication, in: Marine Pollution–Monitoring, Management and Mitigation, Springer, 2023, pp. 75–100.

[16] Z. Wang, Z. Fang, J. Liang, X. Song, Assessment of global habitat suitability and risk of ocean green tides, Harmful Algae 119 (2022) 102324.

[17] P. Miloslavich, N. J. Bax, S. E. Simmons, E. Klein, W. Appeltans, O. Aburto-Oropeza, M. A. Garcia, S. D. Batten, L. Benedetti-Cecchi, D. M. Checkley, S. Chiba, J. E. Duffy, D. C. Dunn, A. Fischer, J. Gunn, R. Kudela, F. Marsac, F. E. Muller-Karger, D. Obura, Y. J. Shin, Essential ocean variables for global sustained observations of biodiversity and ecosystem changes, Global Change Biology 24 (2018) 2416–2433. doi:10.1111/GCB.14108.
URL https://onlinelibrary.wiley.com/doi/full/10.1111/gcb.14108https://onlinelibrary.wiley.com/doi/abs/10.1111/gcb.14108https://onlinelibrary.wiley.com/doi/10.1111/gcb.14108

[18] H. M. Pereira, S. Ferrier, M. Walters, G. N. Geller, R. H. Jongman, R. J. Scholes, M. W. Bruford, N. Brummitt, S. H. Butchart, A. Cardoso, et al., Essential biodiversity variables, Science 339 (6117) (2013) 277–278.

[19] W. Nijland, L. Reshitnyk, E. Rubidge, Satellite remote sensing of canopy-forming kelp on a complex coastline: a novel procedure using the landsat image archive, Remote Sensing of Environment 220 (2019) 41–50.

[20] S. Xu, S. Xu, Y. Zhou, S. Yue, X. Zhang, R. Gu, Y. Zhang, Y. Qiao, M. Liu, Long-term changes in the unique and largest seagrass meadows in the bohai sea (china) using satellite (1974–2019) and sonar data: Implication for conservation and restoration, Remote Sensing 13 (5) (2021) 856.

[21] D. Traganos, P. Reinartz, Mapping mediterranean seagrasses with sentinel-2 imagery, Marine Pollution Bulletin 134 (2018) 197–209. doi:10.1016/j.marpolbul.2017.06.075.

[22] M. M. Coffer, D. D. Graybill, P. J. Whitman, B. A. Schaeffer, W. B. Salls, R. C. Zimmerman, V. Hill, M. C. Lebrasse, J. Li, D. J. Keith, et al., Providing a framework for seagrass mapping in united states coastal ecosystems using high spatial resolution satellite imagery, Journal of Environmental Management 337 (2023) 117669.

[23] B. F. R. Davies, S. Oiry, P. Rosa, M. L. Zoffoli, A. I. Sousa, O. R. Thomas, D. A. Smale, M. C. Austen, L. Biermann, M. J. Attrill, et al., Intertidal seagrass extent from sentinel-2 time-series show distinct trajectories in western europe, Remote Sensing of Environment 312 (2024) 114340.

[24] B. F. R. Davies, S. Oiry, P. Rosa, M. L. Zoffoli, A. I. Sousa, O. R. Thomas, D. A. Smale, M. C. Austen, L. Biermann, M. J. Attrill, et al., A sentinel watching over inter-tidal seagrass phenology across western europe and north africa, Communications Earth & Environment 5 (1) (2024) 382.

[25] P. Ralph, S. Polk, K. Moore, R. Orth, W. Smith Jr, Operation of the xanthophyll cycle in the seagrass zostera marina in response to variable irradiance, Journal of Experimental Marine Biology and Ecology 271 (2) (2002) 189–207.

[26] F. Douay, C. Verpoorter, G. Duong, N. Spilmont, F. Gevaert, New hyperspectral procedure to discriminate intertidal macroalgae, Remote Sensing 14 (2) (2022). doi:10.3390/rs14020346.
URL https://www.mdpi.com/2072-4292/14/2/346

[27] B. F. R. Davies, P. Gernez, A. Geraud, S. Oiry, P. Rosa, M. L. Zoffoli, L. Barillé, Multi- and hyperspectral classification of soft-bottom intertidal vegetation using a spectral library for coastal biodiversity remote sensing, Remote Sensing of Environment 290 (2023) 113554. doi:10.1016/j.rse.2023.113554.
URL https://www.sciencedirect.com/science/article/pii/S0034425723001050

[28] A. Bannari, T. S. Ali, A. Abahussain, The capabilities of sentinel-msi (2a/2b) and landsat-oli (8/9) in seagrass and algae species differentiation using spectral reflectance, Ocean Science 18 (2) (2022) 361–388.

[29] F. Tuya, H. Hernandez-Zerpa, F. Espino, R. Haroun, Drastic decadal decline of the seagrass cymodocea nodosa at gran canaria (eastern atlantic): interactions with the green algae caulerpa prolifera, Aquatic Botany 105 (2013) 1–6.

[30] I. Fairley, B. J. Williamson, J. McIlvenny, N. King, I. Masters, M. Lewis, S. Neill, D. Glasby, D. Coles, B. Powell, et al., Drone-based large-scale particle image velocimetry applied to tidal stream energy resource assessment, Renewable Energy 196 (2022) 839–855.

[31] J. Oh, D.-j. Kim, H. Lee, Use of a drone for mapping and time series image acquisition of tidal zones, Journal of the Korean Institute of Intelligent Systems 27 (2) (2017) 119–125.

[32] R. Adade, A. M. Aibinu, B. Ekumah, J. Asaana, Unmanned aerial vehicle (uav) applications in coastal zone management—a review, Environmental Monitoring and Assessment 193 (2021) 1–12.

[33] E. Casella, J. Drechsel, C. Winter, M. Benninghoff, A. Rovere, Accuracy of sand beach topography surveying by drones and photogrammetry, Geo-Marine Letters 40 (2020) 255–268.

[34] D. B. Angnuureng, K. Brempong, P. Jayson-Quashigah, O. Dada, S. Akuoko, J. Frimpomaa, P. Mattah, R. Almar, Satellite, drone and video camera multi-platform monitoring of coastal erosion at an engineered pocket beach: A showcase for coastal management at elmina bay, ghana (west africa), Regional Studies in Marine Science 53 (2022) 102437.

[35] K. E. Joyce, K. C. Fickas, M. Kalamandeen, The unique value proposition for using drones to map coastal ecosystems, Cambridge Prisms: Coastal Futures 1 (2023) e6.

[36] K. Tallam, N. Nguyen, J. Ventura, A. Fricker, S. Calhoun, J. O'Leary, M. Fitzgibbons, I. Robbins, R. K. Walter, Application of deep learning for classification of intertidal eelgrass from drone-acquired imagery, Remote Sensing 15 (9) (2023) 2321.

[37] M. Roca, M. B. Dunbar, A. Román, I. Caballero, M. L. Zoffoli, P. Gernez, G. Navarro, Monitoring the marine invasive alien species rugulopteryx okamurae using unmanned aerial vehicles and satellites, Frontiers in Marine Science 9 (10 2022). doi:10.3389/fmars.2022.1004012.

[38] A. Román, A. Tovar-Sánchez, I. Olivé, G. Navarro, Using a uav-mounted multispectral camera for the monitoring of marine macrophytes, Frontiers in Marine Science (2021) 1225.

[39] G. Brunier, S. Oiry, Y. Gruet, S. F. Dubois, L. Barillé, Topographic analysis of intertidal polychaete reefs (sabellaria alveolata) at a very high spatial resolution, Remote Sensing 2022, Vol. 14, Page 307 14 (2022) 307. doi:10.3390/RS14020307.
URL https://www.mdpi.com/2072-4292/14/2/307

[40] A. Collin, S. Dubois, D. James, T. Houet, Improving intertidal reef mapping using uav surface, red edge, and near-infrared data, Drones 3 (3) (2019) 67.

[41] T. Rossiter, T. Furey, T. McCarthy, D. B. Stengel, Uav-mounted hyperspectral mapping of intertidal macroalgae, Estuarine, Coastal and Shelf Science 242 (2020) 106789.

[42] M. L. Zoffoli, P. Gernez, P. Rosa, A. Le Bris, V. E. Brando, A.-L. Barillé, N. Harin, S. Peters, K. Poser, L. Spaias, G. Peralta, L. Barillé, Sentinel-2 remote sensing of zostera noltei-dominated intertidal seagrass meadows, Remote Sensing of Environment 251 (2020) 112020. doi:https://doi.org/10.1016/j.rse.2020.112020.
URL https://www.sciencedirect.com/science/article/pii/S0034425720303904

[43] A. I. Sousa, D. B. Santos, E. F. d. Silva, L. P. Sousa, D. F. Cleary, A. M. Soares, A. I. Lillebø, 'blue carbon'and nutrient stocks of salt marshes at a temperate coastal lagoon (ria de aveiro, portugal), Scientific reports 7 (1) (2017) 41225.

[44] B. F. R. Davies, A. I. Sousa, R. Figueira, S. Oiry, P. Gernez, L. Barillé, Benthic intertidal vegetation from the tagus estuary and aveiro lagoon (2023). doi:10.15468/n4ak6x.

[45] C. A. Schneider, W. S. Rasband, K. W. Eliceiri, Nih image to imagej: 25 years of image analysis, Nature methods 9 (7) (2012) 671–675.

[46] Agisoft, Agisoft metashape (2019).
URL https://www.agisoft.com/

[47] S. Nebel, M. Beege, S. Schneider, G. D. Rey, A review of photogrammetry and photorealistic 3d models in education from a psychological perspective, in: Frontiers in education, Vol. 5, Frontiers Media SA, 2020, p. 144.

[48] J. Cao, J. T. Thorson, R. A. Richards, Y. Chen, Spatiotemporal index standardization improves the stock assessment of northern shrimp in the gulf of maine, Canadian Journal of Fisheries and Aquatic Sciences 74 (2017) 1781–1793. doi:10.1139/cjfas-2016-0137.

[49] J. Howard, et al., fastai, https://github.com/fastai/fastai (2018).

[50] P. Wei, Z. Lu, J. Song, Variable importance analysis: A comprehensive review, Reliability Engineering and System Safety 142 (2015) 399–432. doi:https://doi.org/10.1016/j.ress.2015.05.018.
URL https://www.sciencedirect.com/science/article/pii/S0951832015001672

[51] S. Oiry, L. Barillé, Using sentinel-2 satellite imagery to develop microphytobenthos-based water quality indices in estuaries, Ecological Indicators 121 (2021) 107184.

[52] B. K. Veettil, R. D. Ward, M. D. A. C. Lima, M. Stankovic, P. N. Hoai, N. X. Quang, Opportunities for seagrass research derived from remote sensing: A review of current methods, Ecological Indicators 117 (2020) 106560.

[53] T. Christensen, P. S. Dixon, L. M. Irvine, Seaweeds of the british isles: Tribophyceae (xanthophyceae), Vol. 4, British Museum (Natural History), 1977.

[54] P. Cartaxana, S. Cruz, C. Gameiro, M. Kühl, Regulation of intertidal microphytobenthos photosynthesis over a diel emersion period is strongly affected by diatom migration patterns, Frontiers in microbiology 7 (2016) 872.

[55] V. Méléder, M. Laviale, B. Jesus, J. L. Mouget, J. Lavaud, F. Kazemipour, P. Launeau, L. Barillé, In vivo estimation of pigment composition and optical absorption cross-section by spectroradiometry in four aquatic photosynthetic micro-organisms, Journal of Photochemistry and Photobiology B: Biology 129 (2013) 115–124.

[56] A. Bargain, M. Robin, V. Méléder, P. Rosa, E. Le Menn, N. Harin, L. Barillé, Seasonal spectral variation of zostera noltii and its influence on pigment-based vegetation indices, Journal of experimental marine biology and ecology 446 (2013) 86–94.

[57] K. Beach, H. Borgeas, N. Nishimura, C. Smith, In vivo absorbance spectra and the ecophysiology of reef macroalgae, Coral Reefs 16 (1997) 21–28.

[58] J. T. Kirk, Light and photosynthesis in aquatic ecosystems, Cambridge university press, 1994.

[59] J. D. Hedley, M. Mirhakak, A. Wentworth, H. M. Dierssen, Influence of three-dimensional coral structures on hyperspectral benthic reflectance and water-leaving reflectance, Applied Sciences 8 (12) (2018) 2688.

[60] T. Repolho, B. Duarte, G. Dionísio, J. R. Paula, A. R. Lopes, I. C. Rosa, T. F. Grilo, I. Caçador, R. Calado, R. Rosa, Seagrass ecophysiological performance under ocean warming and acidification, Scientific Reports 7 (1) (2017) 41443.

[61] B. Charrier, S. Boscq, B. J. Nelson, N. F. Läubli, Growth and labelling of cell wall components of the brown alga ectocarpus in microfluidic chips, Frontiers in Marine Science 8 (2021) 745654.

[62] M. R. Slaton, E. Raymond Hunt Jr., W. K. Smith, Estimating near-infrared leaf reflectance from leaf structural characteristics, American Journal of Botany 88 (2) (2001) 278–284. arXiv:https://bsapubs.onlinelibrary.wiley.com/doi/pdf/10.2307/2657019, doi:https://doi.org/10.2307/2657019.
URL https://bsapubs.onlinelibrary.wiley.com/doi/abs/10.2307/2657019

[63] European-Commission, "DIRECTIVE 2000/60/EC OF THE EUROPEAN PARLIAMENT AND OF THE COUNCIL of 23 October 2000 establishing a framework for Community action in the field of water policy" or, in short, the EU Water Framework Directive, Official Journal of the European Communities L 327 (1) (2000) 1–72.

[64] B. Légaré, S. Bélanger, R. K. Singh, P. Bernatchez, M. Cusson, Remote sensing of coastal vegetation phenology in a cold temperate intertidal system: implications for classification of coastal habitats, Remote Sensing 14 (13) (2022) 3000.

[65] S. Fyfe, Spatial and temporal variation in spectral reflectance: Are seagrass species spectrally distinct?, Limnology and Oceanography 48 (1part2) (2003) 464–479.

[66] V. Costa, J. Serôdio, A. I. Lillebø, A. I. Sousa, Use of hyperspectral reflectance to non-destructively estimate seagrass zostera noltei biomass, Ecological Indicators 121 (2021) 107018. doi:https://doi.org/10.1016/j.ecolind.2020.107018. URL https://www.sciencedirect.com/science/article/pii/S1470160X20309572

[67] E. Piaser, A. Berton, R. Bolpagni, M. Caccia, M. B. Castellani, A. Coppi, A. Dalla Vecchia, F. Gallivanone, G. Sona, P. Villa, Impact of radiometric variability on ultra-high resolution hyperspectral imagery over aquatic vegetation: preliminary results, IEEE Journal of Selected Topics in Applied Earth Observations and Remote Sensing (2023).

[68] A. Schibalski, M. Kleyer, M. Maier, B. Schröder, Spatiotemporally explicit prediction of future ecosystem service provisioning in response to climate change, sea level rise, and adaptation strategies, Ecosystem Services 54 (2022) 101414. doi:https://doi.org/10.1016/j.ecoser.2022.101414. URL https://www.sciencedirect.com/science/article/pii/S2212041622000109

[69] F. Holon, G. Marre, V. Parravicini, N. Mouquet, T. Bockel, P. Descamp, A.-S. Tribot, P. Boissery, J. Deter, A predictive model based on multiple coastal anthropogenic pressures explains the degradation status of a marine ecosystem: Implications for management and conservation, Biological Conservation 222 (2018) 125–135.

[70] P. A. Marquet, A. H. Buschmann, D. Corcoran, P. A. Díaz, T. Fuentes-Castillo, R. Garreaud, P. Pliscoff, A. Salazar, Global change and acceleration of anthropic pressures on patagonian ecosystems, in: Conservation in Chilean Patagonia: Assessing the State of Knowledge, Opportunities, and Challenges, Springer International Publishing Cham, 2024, pp. 33–65.

[71] F. E. Muller-Karger, E. Hestir, C. Ade, K. Turpie, D. A. Roberts, D. Siegel, R. J. Miller, D. Humm, N. Izenberg, M. Keller, et al., Satellite sensor requirements for monitoring essential biodiversity variables of coastal ecosystems, Ecological applications 28 (3) (2018) 749–760.

[72] P. Villalobos Perna, M. Di Febbraro, M. L. Carranza, F. Marzialetti, M. Innangi, Remote sensing and invasive plants in coastal ecosystems: What we know so far and future prospects, Land 12 (2) (2023) 341.

[73] M. A. Sutton, H. Van Grinsven, G. Billen, A. Bleeker, A. Bouwman, O. Oenema, European nitrogen assessement-summary for policy makers, in: the European Nitrogen Assessment. Sources, Effects and Policy Perspectives, 2011, pp. xxiv–xxxiv.

[74] N.-h. Ye, X.-w. Zhang, Y.-z. Mao, C.-w. Liang, D. Xu, J. Zou, Z.-m. Zhuang, Q.-y. Wang, 'green tides' are overwhelming the coastline of our blue planet: taking the world's largest example, Ecological Research 26 (2011) 477–485.

[75] R. Villares, X. Puente, A. Carballeira, Nitrogen and phosphorus in ulva sp. in the galician rias bajas (northwest spain): Seasonal fluctuations and influence on growth, Boletin-Instituto Español de Oceanografia 15 (1/4) (1999) 337–342.

[76] A. Ménesguen, Les marées vertes: 40 clés pour comprendre, Editions Quae, 2018.

[77] C. Louime, J. Fortune, G. Gervais, Sargassum invasion of coastal environments: a growing concern, American Journal of Environmental Sciences 13 (1) (2017) 58–64.

[78] L. Schreyers, T. van Emmerik, L. Biermann, Y.-F. Le Lay, Spotting green tides over brittany from space: Three decades of monitoring with landsat imagery, Remote Sensing 13 (8) (2021). doi:10.3390/rs13081408. URL https://www.mdpi.com/2072-4292/13/8/1408

[79] V. Klemas, Remote sensing of algal blooms: an overview with case studies, Journal of coastal research 28 (1A) (2012) 34–43.

[80] S. Haro, J. Jimenez-Reina, R. Bermejo, L. Morrison, Biointertidal mapper software: A satellite approach for ndvi-based intertidal habitat mapping, SoftwareX 24 (2023) 101520.

[81] E. Papathanasopoulou, S. Simis, K. Alikas, A. Ansper, J. Anttila, A. Barillé, L. Barillé, V. Brando, M. Bresciani, M. Bučas, et al., Satellite-assisted monitoring of water quality to support the implementation of the water framework directive, EOMORES white paper (2019).

[82] L. Ratnarajah, R. Abu-Alhaija, A. Atkinson, S. Batten, N. J. Bax, K. S. Bernard, G. Canonico, A. Cornils, J. D. Everett, M. Grigoratou, et al., Monitoring and modelling marine zooplankton in a changing climate, Nature Communications 14 (1) (2023) 564.

[83] J. Foden, D. Brazier, Angiosperms (seagrass) within the eu water framework directive: a uk perspective, Marine Pollution Bulletin 55 (1-6) (2007) 181–195.

[84] L. M. Nordlund, R. K. Unsworth, S. Wallner-Hahn, L. Ratnarajah, P. Beca-Carretero, E. Boikova, J. C. Bull, R. M. Chefaoui, C. B. de los Santos, K. Gagnon, et al., One hundred priority questions for advancing seagrass conservation in europe, Plants, People, Planet (2024).